Scripta Materialia 191 (2021) 29–33

Contents lists available at ScienceDirect

Scripta Materialia

journal homepage: www.elsevier.com/locate/scriptamat

Predicting single phase stability and segregation in the NbMoTaTi–(W,V) high entropy alloy system with the vacancy exchange potential

Samuel W. McAlpine*, Julie V. Logan, Michael P. Short

Department of Nuclear Science and Engineering Massachusetts Institute of Technology 77 Massachusetts Avenue Cambridge, MA 02139, United States

ARTICLE INFO

Article history:
Received 28 May 2020
Revised 20 August 2020
Accepted 22 August 2020

Keywords:
High entropy alloys
Refractory metals
Ab initio calculation
Vacancies
Casting

ABSTRACT

High entropy alloys (HEAs) are potential next-generation structural materials, yet accurate prediction of phase stability remains a challenge. We study two equimolar refractory high entropy alloys, NbMoTaTi–X (X = W, V). *Ab initio* calculations are performed to determine the vacancy exchange potential in both alloys. Results and experimental confirmation indicate that a zero/low vacancy exchange potential predicts phase instability in NbMoTaTiW, while elemental trends of the same predict segregation in single phase NbMoTaTiV. If these results hold true across other systems, vacancy exchange potential can serve as a rapid predictor of stability in the vast HEA compositional space.

For centuries, alloy design has consisted of the selection of one or more principal elements, with other elements added in small concentrations to optimize particular properties such strength, toughness, or corrosion resistance. High entropy alloys (HEAs), also known as multi–principal element alloys, represent a different and useful design paradigm in metallurgy and materials science. Instead of beginning with a single base element and adding a variety of alloying elements, HEAs have compositions of at least 4 principal elements, often in equimolar proportion [38]. Although part of the motivation underlying the study of HEAs is the formation of a single, thermodynamically stable phase in order to suppress embrittling intermetallics, multiphase materials in high entropy systems can be beneficial due to precipitation strengthening [8,16,18,28]. HEAs based on 3*d* transition metals have received the bulk of the attention in the research community over the past decade [22]. In contrast, HEAs composed of refractory metals such as Nb, Mo, W, etc. have received relatively little attention until recently [5,22]. While this HEA subgroup is less mature, refractory HEAs (RHEAs) could potentially serve as next–generation structural materials for high temperature applications such as gas turbines or advanced nuclear energy systems, particularly nuclear fusion reactors [9,11,25,29].

Much effort has gone into determining which HEA compositions tend to form a single phase solid solution [12,13,19,30,31,39]. Along with the formation of a single solid solution, possible equilibrium states can include multiple solid solutions, spinodal decomposition, and intermetallic precipitate formation. Recently, there has been a focus on the use of computational techniques such as first–principles electronic structure calculations to screen the huge HEA compositional space available to determine which compositions form single phase solid solutions. Both HEA compositions studied in this work, equimolar NbMoTaTiW and NbMoTaTiV, are predicted to form single phase body–center cubic (BCC) solid solutions by Troparevsky et al. [31], as well as by the Alloy Search and Predict (ASAP) tool developed by King et al. [1,12,13].

Vacancy behavior is also important due to their involvement in a variety of material processes such as solid state diffusion, high temperature creep deformation, and radiation damage. The information available in the literature concerning vacancy behavior in HEAs is sparse, which is likely due to the difficulty in determining the vacancy formation energy in complex solid solutions. In pure monatomic crystals, a single vacancy formation energy (VFE) is sufficient to describe the system at a given temperature because all of the sites in the crystal are symmetrically equivalent. Using atomistic simulation, the VFE of a pure material can be obtained by comparing the energy of a pristine supercell of N atoms with zero vacancies, $E(N, 0)$, and a supercell with a single atom removed in

* Corresponding author.
E-mail addresses: alloy94@mit.edu, samuel.w.mcalpine@gmail.com (S.W. McAlpine).

https://doi.org/10.1016/j.scriptamat.2020.08.043
1359-6462/

order to form a vacancy, $E(N-1,1)$, accounting for the different number of atoms in each case [20]:

$$E^{\mathrm{f}}_{\mathrm{Va}} = E(N-1,1) - \frac{N-1}{N}E(N,0) \quad (1)$$

In contrast, in highly chemically complex crystalline systems like HEAs, each site in the crystal can have a varying local atomic environment. Therefore, instead of a single vacancy formation energy to describe the system, a distribution of vacancy formation energies is required, as a function of the local environment of the vacancy. A similar calculation can be performed for a HEA by removing an atom, but one must properly account for the effect of changing the composition of the supercell by introducing a chemical potential term [37]:

$$E(N-1,1) - \frac{N-1}{N}E(N,0) = E^{\mathrm{f}}_{\mathrm{Va}_i^j} - \mu_i \quad (2)$$

where Va_i^j indicates that an atom of type i was removed from site j in the supercell to create a vacancy, and μ_i is the chemical potential of element i within the HEA. In practice, the determination of the chemical potential of each component in a HEA is very challenging. Methods such as the cluster expansion (CE) technique have been used for binary and ternary alloys [3,33,37], but for systems of more than 3 components the number of effective cluster interactions which must be included in the expansion leads to a prohibitively high computational cost. Therefore, we define a vacancy exchange potential $\tilde{\mu}_{\mathrm{Va}_i^j}$ in the same manner as Belak and Van der Ven [3]:

$$\tilde{\mu}_{\mathrm{Va}_i^j} = E^{\mathrm{f}}_{\mathrm{Va}_i^j} - \mu_i \quad (3)$$

Although this quantity alone will not allow for the determination of the VFE distribution, useful insights may still be extracted from the behavior and trends of the vacancy exchange potential [3]. The VFE should be independent of the atom type which occupies the vacant site in the pristine supercell because the system has no memory of the atom which occupied the site. The VFE should depend only on the local atomic configuration surrounding the vacancy [26]. Therefore, differences in the vacancy exchange potential between different components of the alloy are primarily attributable to differences in chemical potential between the components.

In this work, we employ *ab initio* calculations to obtain the distribution of vacancy exchange potentials for each element in equiatomic BCC NbMoTaTi–(W, V) solid solution HEAs at 0 K. In addition, the NbMoTaTi–(W,V) HEAs are synthesized using the arc melting technique, followed by characterization using scanning electron microscopy (SEM), energy dispersive X–ray spectroscopy (EDX), and X–ray diffraction (XRD). We show the relationship between vacancy exchange potential, phase stability, and elemental segregation, with results implicating that vacancy exchange potential could be a simple, yet powerful tool to predict phase stability and segregation behavior in complex alloys such as HEAs. In particular, we find that the mean vacancy exchange potential of Ti in NbMoTaTiW is approximately zero. Upon casting, this HEA undergoes phase separation into two solid solution phases, one of which is Ti–rich with an HCP structure and another which is W–rich with a BCC structure.

Non–spin polarized first–principles density functional theory (DFT) calculations were conducted using the Vienna *Ab initio* Simulation Package (VASP) [6,14]. A plane–wave cutoff energy of 600 eV was used throughout the calculations, along with a Γ–centered 7x7x7 k–point grid to sample the Brillouin zone. The total energy of the pristine supercell was found to converge to within 5 meV under these conditions. The projector augmented–wave (PAW) pseudopotentials were used to describe the ion–electron interactions [4,15]. The Perdew–Burke–Ernzerhof parameterization of the generalized gradient approximation (GGA) exchange–correlation

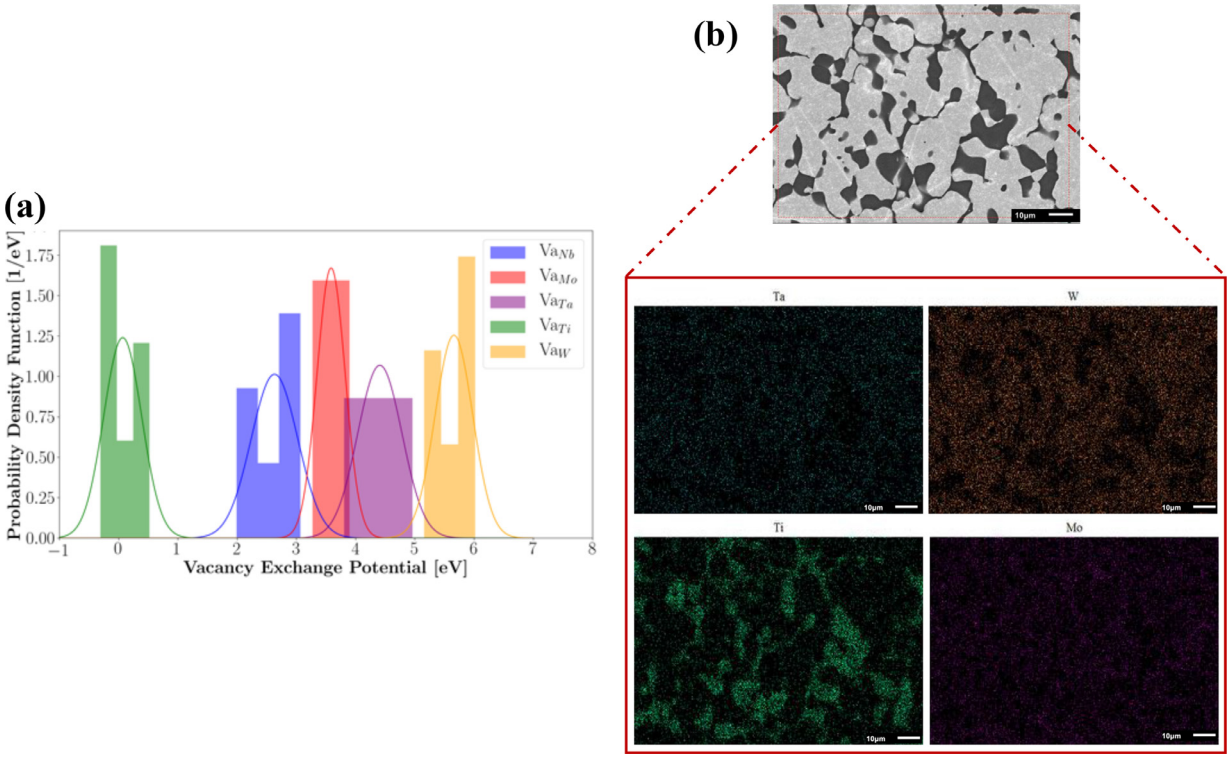

Fig. 1. (a) Vacancy exchange potential distribution in NbMoTaTiW. A normal distribution fit for each element is also shown. (b) SEM image of NbMoTaTiW HEA, along with EDX intensity maps for Ta, Mo, Ti and W. There are two distinct phases, one which appears dark in the SEM image and is rich in Ti, and the other bright in the SEM image and rich in W.

functional, revised for use in solids (PBEsol) was used [23,24]. Additionally, relaxation of the supercell size, shape, and ionic positions was performed for both the pristine and vacancy–containing structures to account for the effect of local lattice distortion.

In order to physically represent the random solid solution HEAs, the sequential quasirandom structure (SQS) method was employed [40]. The SQS method has been shown to accurately predict the properties of disordered solids with supercells as small as 16 atoms [10,17,27,35,36]. Distinct 30 atom SQS supercells for both alloys were produced using the `mcsqs` code within the Alloy Theoretic Automated Toolkit [32,34]. Please see the Supplementary Materials for more details about SQS generation and larger 125 atom simulations conducted for validation purposes. The SQS method differs from other popular methods for representing random solid solutions such as the coherent potential approximation (CPA) and the virtual crystal approximation (VCA) in that it is not an effective medium approach, and therefore the SQS method can provide detailed insights into the effect of local atomic structure within random solid solutions.

To better understand both RHEAs and connect the results of the calculations with the physical structure of the alloys, we experimentally synthesize both RHEA compositions. Elemental powders (99.9% purity or greater) purchased from Alfa Aesar are vacuum pressed into 25 gram pellets and cast. Samples are melted in an arc melter (Centorr Vacuum Industries Model 5SA) within an ultrapure (99.999% pure Ar) inert atmosphere following a pump–and–purge procedure to maximize atmosphere purity. The arc melter utilizes a copper hearth cooled by chilled water upon which the molten RHEAs solidify. After the initial casting, the samples are removed, flipped, and remelted three times in order to enhance sample homogeneity.

After arc melting, the as–cast RHEAs are sectioned using a low–speed saw and mechanically polished using SiC polishing paper to 1200 grit and 1 µm diamond particle suspension. The samples are imaged using a JEOL 6610 SEM equipped with EDX to enable elemental identification and quantification. A Bruker D8 Discover General Area Detector Diffraction System (GADDS) employing a 1.6 kW sealed tube cobalt anode and Vantec-2000 two-dimensional detector is used to acquire the XRD spectra. These are acquired with sample rotation and scan axis oscillation to ensure that the data obtained are representative of the sample at large.

Fig. 1 (a) shows the estimated vacancy exchange potential probability density function (PDF) in BCC NbMoTaTiW. Half of the Ti sites in the 30 atom NbMoTaTiW SQS have negative vacancy exchange potential values, and the mean vacancy exchange potential for Va_{Ti} is 0.07 eV. A negative vacancy exchange potential suggests inherent thermodynamic instability at 0 K for the Ti atomic sites within BCC NbMoTaTiW as it indicates an energetic preference for a vacant site instead of a Ti atom occupying that site.

An SEM micrograph of as–cast NbMoTaTiW is shown in Fig. 1(b), along with EDX elemental maps. Two regions are present, a dark region rich in Ti and a bright region rich in W. Ta is more concentrated in the bright region, whereas Nb and Mo are relatively evenly distributed between the two regions.

The vacancy exchange potential distribution for NbMoTaTiV is shown in Fig. 2(a). In this case, the VFE among Ti sites is higher than in NbMoTaTiW, and the spread in vacancy exchange potential among the different elements is smaller due to the absence of W. A low–magnification SEM image of as–cast NbMoTaTiV is shown in Fig. 2(b), along with EDX elemental maps of Ta, Ti, and V. The as–cast sample has a dendritic/cellular microstructure, with the dark dendrites being rich in Ti and V and the brighter interdentritic region rich in Ta. A higher magnification SEM image of NbMoTaTiV is shown in Fig. 3. At higher magnification the microstructure appears cellular, with an EDX linescan showing that the dark boundaries are indeed enriched in Ti and V, while depleted in Ta. Nb

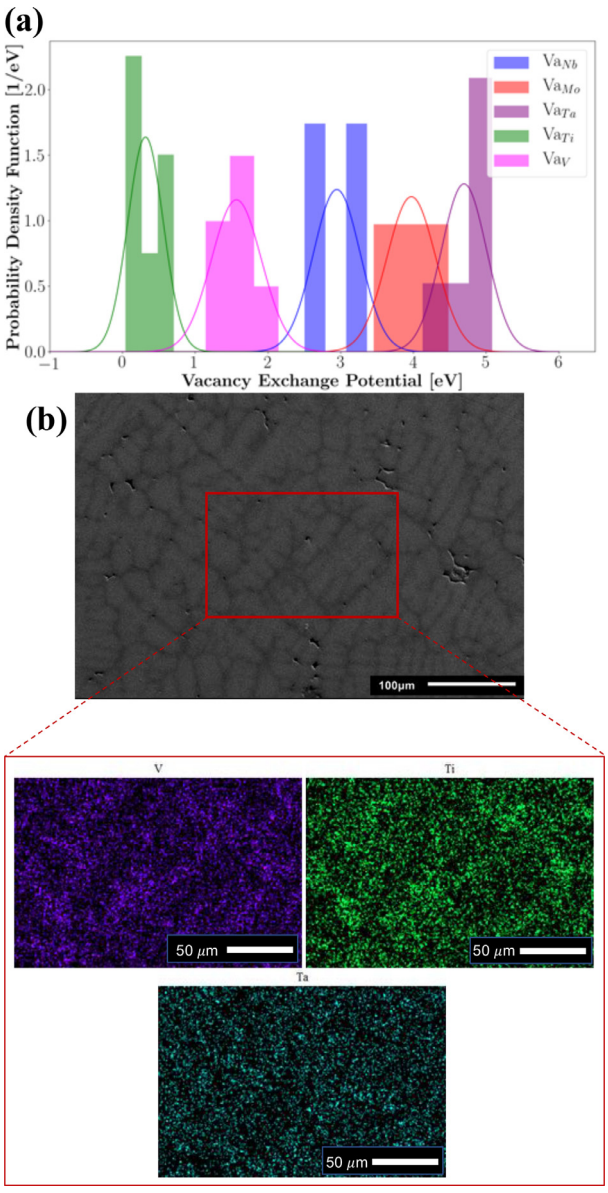

Fig. 2. (a) Vacancy exchange potential distribution in NbMoTaTiV. The data for each element is fit with a normal distribution, which is also shown. (b) SEM image of as–cast microstructure of NbMoTaTiV HEA, with EDX elemental maps for Ta, Ti, and V.

does not segregate into either the cell boundary region or within the cells, while the segregation of Mo is relatively small.

XRD patterns of the as–cast NbMoTaTiW and NbMoTaTiV RHEAs are shown in Fig. 4(a). The XRD patterns show a dual phase BCC + HCP structure in the as–cast NbMoTaTiW RHEA, while the as–cast NbMoTaTiV RHEA has a single phase BCC structure. The dark Ti–rich phase in Fig. 1(b) is likely HCP while the bright W–rich phase corresponds to the BCC phase.

In order to quantify the degree of segregation in NbMoTaTiV, a ratio of the concentration in the dendrite region and the interdendritic region $C_{\text{den}}/C_{\text{int}}$ is calculated for each elemental component in NbMoTaTiV, shown in Fig. 4(b), plotted against the mean vacancy exchange potential $\langle\tilde{\mu}_{\text{Va}}\rangle$. This plot shows a strong correlation between the vacancy exchange potential of the elements in the HEA and the degree to which those elements tend to segregate upon casting. Elements, such as Ti and V, with lower vacancy exchange potentials, tend to become enriched in the dendritic region. Conversely, elements such as Ta with a higher vacancy ex-

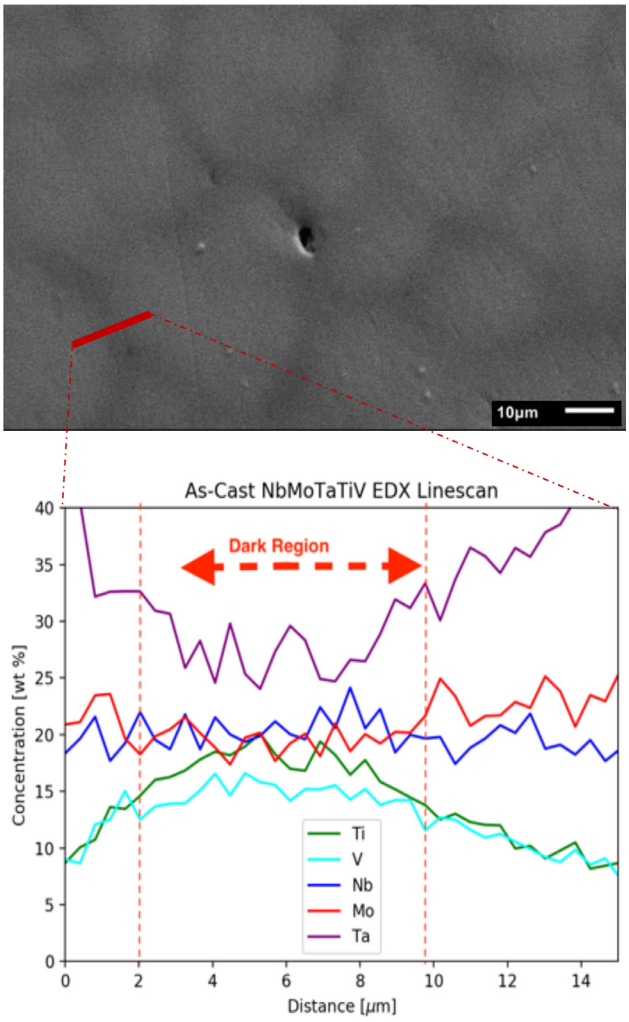

Fig. 3. 1,000X magnification SEM image of as–cast NbMoTaTiV along with EDX linescan showing Ti/V enrichment and Ta depletion in the dark, dendritic region. The solid red bar indicates the linescan path.

change potential tend to become depleted in the dendritic region and enriched in the interdendritic region.

The most notable aspect of our results is the fact that the obtained mean vacancy exchange potential for Ti in BCC NbMoTaTiW (0.07 eV) is very close to zero, with half the sites having negative vacancy exchange potential values. This implies the chemical potential of Ti in the NbMoTaTiW BCC HEA is approximately equal to the vacancy formation energy at 0 K. Upon casting NbMoTaTiW forms a Ti–rich HCP phase, indicating that Ti is indeed not thermodynamically stable in the equimolar NbMoTaTiW BCC structure at room temperature, even though this composition is predicted by several methods to be a single phase BCC structure [1,12,13,31]. Unlike NbMoTaTiW, NbMoTaTiV does form a single phase BCC structure upon casting, while the mean vacancy exchange potential of Ti is 0.32 eV, significantly greater than in NbMoTaTiW. Therefore, a mean vacancy exchange potential near zero could be indicative of a tendency for phase separation in HEAs. Furthermore, the large difference in vacancy exchange potential between Ti and W in NbMoTaTiW compared to the small difference in vacancy exchange potential between Ti and V in NbMoTaTiV might be an indication of why replacing W with V leads to single phase BCC stability.

Han et al. reported the as–cast microstructures of NbMoTaTi$_x$W–type HEAs, including equimolar NbMoTaTiW [7]. They report single phase BCC crystal structure for NbMoTaTiW, which is in disagreement with our finding of a dual phase BCC + HCP structure for NbMoTaTiW. But, in their study they also report calculated phase diagrams obtained from Thermo–Calc [2] using the TTNI 8 database. In these calculated phase diagrams, HCP appears as one of the stable phases in NbMoTaTiW below approximately 800°C. One possible explanation for the difference in our results is that in their casting procedure, cooling may have occurred so quickly that the HCP phase was unable to nucleate and grow, resulting in just BCC being present in the as–cast microstructure.

Upon casting NbMoTaTiV did exhibit a dendritic microstructure with elemental segregation. Again, there is a connection to the vacancy exchange potential. Elements with comparatively low vacancy exchange potentials tend to concentrate within or near dendrite arms, while elements with relatively high vacancy exchange potential tend to become enriched in the interdendritic region.

In summary, we have shown that the vacancy exchange potential has the potential to be a powerful tool for prediction of phase stability and elemental segregation in complex solid solutions such as HEAs. We use *ab initio* calculations to predict the vacancy exchange potential in NbMoTaTiV and NbMoTaTiW. Because both of these compositions are predicted to be single phase BCC alloys by multiple sources, we model them as BCC random solid solutions using the SQS method. We find that half of Ti sites in NbMoTaTiW have a negative vacancy exchange potential, unlike NbMoTaTiV, indicating some degree of thermodynamic instability for BCC NbMoTaTiW. Subsequent experimental study of the microstructure and phase stability of these alloys indicates a dual phase BCC + HCP structure for NbMoTaTiW, while NbMoTaTiV has a single phase BCC structure. In single phase NbMoTaTiV, we find that there is a

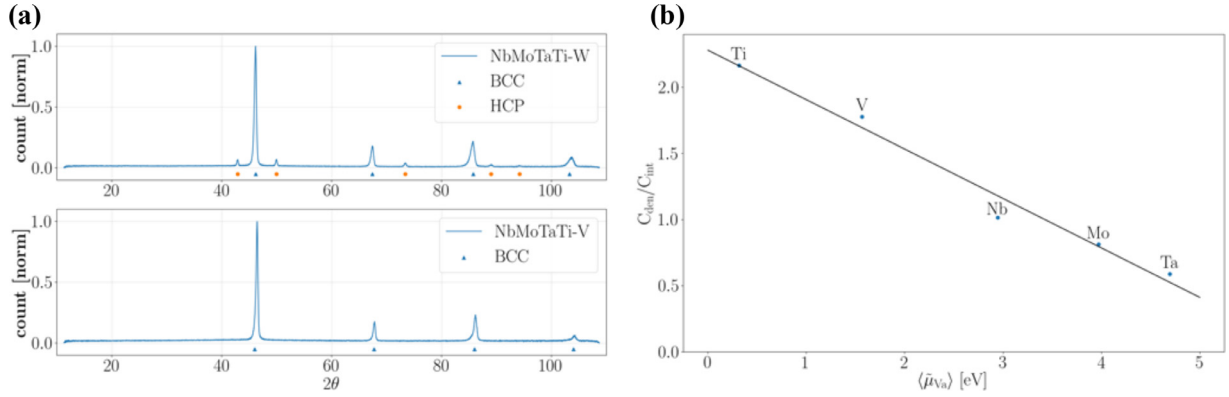

Fig. 4. (a) XRD patterns of NbMoTaTiW and NbMoTaTiV. NbMoTaTiW demonstrates peaks indicative of the presence of both BCC and HCP phases, while NbMoTaTiV demonstrates only BCC diffraction peaks. (b) Plot of segregation ratio C_{den}/C_{int} vs. the mean vacancy exchange potential $\langle\tilde{\mu}_{Va}\rangle$ for each element within the NbMoTaTiV alloy.

connection between the vacancy exchange potential and elemental segregation upon casting, with elements that have a lower vacancy exchange potential in the alloy tending to become enriched in the dendritic region and elements which have a higher vacancy exchange potential tending to become enriched in the interdendritic region. Therefore, the vacancy exchange potential as predicted by *ab initio* calculations can be used as an indicator of phase stability and elemental segregation and merits further study as a potential tool for computational screening of phase stability and segregation in high entropy alloys.

Data availability

The raw/processed data required to reproduce these findings are available at [21].

Declaration of Competing Interest

The authors declare that they have no known competing financial interests or personal relationships that could have appeared to influence the work reported in this paper.

Acknowledgments

SWM would like to acknowledge the support of the Nuclear Regulatory Commission through a Graduate Fellowship. This research did not receive any specific grant from funding agencies in the public, commercial, or not-for-profit sectors.

Supplementary material

Supplementary material associated with this article can be found, in the online version, at doi:10.1016/j.scriptamat.2020.08.043

References

[1] Alloy search and predict, 2016, (http://www.alloyasap.com).
[2] J.-O. Andersson, T. Helander, L. Höglund, P. Shi, B. Sundman, Calphad 26 (2) (2002) 273–312.
[3] A.A. Belak, A. Van der Ven, Phys. Rev. B 91 (22) (2015) 224109.
[4] P.E. Blöchl, Phys. Rev. B 50 (24) (1994) 17953.
[5] E.P. George, D. Raabe, R.O. Ritchie, Nat. Rev. Mater. 4 (8) (2019) 515–534.
[6] J. Hafner, J. Comput. Chem. 29 (13) (2008) 2044–2078.
[7] Z. Han, H. Luan, X. Liu, N. Chen, X. Li, Y. Shao, K. Yao, Mater. Sci. Eng. 712 (2018) 380–385.
[8] J. He, H. Wang, H. Huang, X. Xu, M. Chen, Y. Wu, X. Liu, T. Nieh, K. An, Z. Lu, Acta Mater. 102 (2016) 187–196.
[9] E.-W. Huang, P.K. Liaw, MRS Bull. 44 (11) (2019) 847–853, doi:10.1557/mrs.2019.257.
[10] C. Jiang, Acta Mater. 57 (16) (2009) 4716–4726.
[11] A. Kareer, J. Waite, B. Li, A. Couet, D. Armstrong, A. Wilkinson, J. Nucl. Mater. 526 (2019) 151744.
[12] D. King, S. Middleburgh, L. Edwards, G. Lumpkin, M. Cortie, JOM 67 (10) (2015) 2375–2380.
[13] D. King, S. Middleburgh, A. McGregor, M. Cortie, Acta Mater. 104 (2016) 172–179.
[14] G. Kresse, J. Furthmüller, Comput. Mater. Sci 6 (1) (1996) 15–50.
[15] G. Kresse, D. Joubert, Phys. Rev. B 59 (3) (1999) 1758.
[16] W. Liu, Z. Lu, J. He, J. Luan, Z. Wang, B. Liu, Y. Liu, M. Chen, C. Liu, Acta Mater. 116 (2016) 332–342.
[17] Z. Liu, B.P. Burton, S. Khare, D. Gall, J. Phys. 29 (3) (2016) 035401.
[18] Y. Lu, Y. Dong, S. Guo, L. Jiang, H. Kang, T. Wang, B. Wen, Z. Wang, J. Jie, Z. Cao, et al., Sci. Rep. 4 (2014) 6200.
[19] H.-W. Luan, Y. Shao, J.-F. Li, W.-L. Mao, Z.-D. Han, C. Shao, K.-F. Yao, Scr. Mater. 179 (2020) 40–44.
[20] T.R. Mattsson, A.E. Mattsson, Phys. Rev. B 66 (21) (2002) 214110.
[21] S.W. McAlpine, J.V. Logan, M.P. Short, NbMoTaTi(W,V) refractory HEA data, 2020, (https://doi.org/10.5281/zenodo.3861011).
[22] D. Miracle, O. Senkov, Acta Mater. 122 (2017) 448–511.
[23] J.P. Perdew, K. Burke, M. Ernzerhof, Phys. Rev. Lett. 77 (18) (1996) 3865.
[24] J.P. Perdew, A. Ruzsinszky, G.I. Csonka, O.A. Vydrov, G.E. Scuseria, L.A. Constantin, X. Zhou, K. Burke, Phys. Rev. Lett. 100 (13) (2008) 136406.
[25] S. Praveen, H.S. Kim, Adv. Eng. Mater. 20 (1) (2018) 1700645.
[26] A.V. Ruban, Phys. Rev. B 93 (13) (2016) 134115.
[27] J.E. Saal, C. Wolverton, Acta Mater. 61 (7) (2013) 2330–2338.
[28] L. Santodonato, Y. Zhang, M. Feygenson, C. Parish, M. Gao, R. Weber, J. Neufeind, Z. Tang, P. Liaw, Nat. Commun. 6 (2015) 5964.
[29] O. Senkov, S. Gorsse, D. Miracle, Acta Mater. 175 (2019) 394–405.
[30] O. Senkov, J. Miller, D. Miracle, C. Woodward, Nat. Commun. 6 (1) (2015) 1–10.
[31] M. Troparevsky, J. Morris, P. Kent, A. Lupini, G. Stocks, Phys. Rev. X 5 (1) (2015) 011041.
[32] A. Van De Walle, Calphad 33 (2) (2009) 266–278.
[33] A. Van der Ven, G. Ceder, Phys. Rev. B 71 (5) (2005) 054102.
[34] A. Van de Walle, P. Tiwary, M. De Jong, D. Olmsted, M. Asta, A. Dick, D. Shin, Y. Wang, L.-Q. Chen, Z.-K. Liu, Calphad 42 (2013) 13–18.
[35] Y. Wang, M. Yan, Q. Zhu, W.Y. Wang, Y. Wu, X. Hui, R. Otis, S.-L. Shang, Z.-K. Liu, L.-Q. Chen, Acta Mater. 143 (2018) 88–101.
[36] C. Wolverton, Acta Mater. 49 (16) (2001) 3129–3142.
[37] X. Zhang, M.H. Sluiter, Phys. Rev. B 91 (17) (2015) 174107.
[38] Y. Zhang, T. Zuo, Z. Tang, M. Gao, K. Dahmen, P. Liaw, Z. Lu, Prog. Mater Sci. 61 (2014) 1–93.
[39] Z. Zhou, Y. Zhou, Q. He, Z. Ding, F. Li, Y. Yang, npj Comput. Mater. 5 (1) (2019) 1–9.
[40] A. Zunger, S.-H. Wei, L. Ferreira, J.E. Bernard, Phys. Rev. Lett. 65 (3) (1990) 353.